Upregulation of the Phthiocerol Dimycocerosate Biosynthetic Pathway by Rifampin-Resistant, *rpoB* Mutant *Mycobacterium tuberculosis*

Gregory P. Bisson,[a,b] Carolina Mehaffy,[c] Corey Broeckling,[d] Jessica Prenni,[d] Dalin Rifat,[e] Desmond S. Lun,[f,g] Marcos Burgos,[h] Drew Weissman,[a] Petros C. Karakousis,[e] and Karen Dobos[c]

Division of Infectious Diseases, Department of Medicine, The Perelman School of Medicine at the University of Pennsylvania, Philadelphia, Pennsylvania, USA[a]; Center for Clinical Epidemiology and Biostatistics, The Perelman School of Medicine at the University of Pennsylvania, Philadelphia, Pennsylvania, USA[b]; Department of Microbiology, Immunology, and Pathology[c] and Proteomics and Metabolomics Facility,[d] Colorado State University, Fort Collins, Colorado, USA; Center for Tuberculosis Research, Johns Hopkins University School of Medicine, Baltimore, Maryland, USA[e]; Center for Computational and Integrative Biology and Department of Computer Science, Rutgers University, Camden, New Jersey, USA[f]; Phenomics and Bioinformatics Research Centre and School of Mathematics and Statistics, University of South Australia, Mawson Lakes, South Australia, Australia[g]; and Department of Internal Medicine, Division of Infectious Diseases, University of New Mexico, Albuquerque, New Mexico, USA[h]

Multidrug-resistant tuberculosis has emerged as a major threat to tuberculosis control. Phylogenetically related rifampin-resistant actinomycetes with mutations mapping to clinically dominant *Mycobacterium tuberculosis* mutations in the *rpoB* gene show upregulation of gene networks encoding secondary metabolites. We compared the expressed proteomes and metabolomes of two fully drug-susceptible clinical strains of *M. tuberculosis* (wild type) to those of their respective rifampin-resistant, *rpoB* mutant progeny strains with confirmed rifampin monoresistance following antitubercular therapy. Each of these strains was also used to infect gamma interferon- and lipopolysaccharide-activated murine J774A.1 macrophages to analyze transcriptional responses in a physiologically relevant model. Both *rpoB* mutants showed significant upregulation of the polyketide synthase genes *ppsA-ppsE* and *drrA*, which constitute an operon encoding multifunctional enzymes involved in the biosynthesis of phthiocerol dimycocerosate and other lipids in *M. tuberculosis*, but also of various secondary metabolites in related organisms, including antibiotics, such as erythromycin and rifamycins. *ppsA* (Rv2931), *ppsB* (Rv2932), and *ppsC* (Rv2933) were also found to be upregulated more than 10-fold in the Beijing *rpoB* mutant strain relative to its wild-type parent strain during infection of activated murine macrophages. In addition, metabolomics identified precursors of phthiocerol dimycocerosate, but not the intact molecule itself, in greater abundance in both *rpoB* mutant isolates. These data suggest that *rpoB* mutation in *M. tuberculosis* may trigger compensatory transcriptional changes in secondary metabolism genes analogous to those observed in related actinobacteria. These findings may assist in developing novel methods to diagnose and treat drug-resistant *M. tuberculosis* infections.

Approximately 9 million people develop active tuberculosis (TB) each year, resulting in nearly 2 million deaths annually (75). Recent progress controlling drug-susceptible TB has been made in many regions (50); however, drug resistance in *Mycobacterium tuberculosis*, including strains resistant to both first-line drugs, isoniazid and rifampin (multidrug-resistant [MDR] TB), has emerged as a threat to TB control worldwide (26, 65). Although international surveillance systems are inadequate, data from over 80 countries indicate that approximately 1 in 10 new cases of active TB have primary drug resistance (77), and MDR TB has been reported in essentially every country in which drug resistance has been studied (76). Treatment of MDR TB requires the use of costly and toxic second-line drugs for nearly 2 years and is associated with high rates of morbidity and mortality (65), which makes the spread of drug-resistant TB a major public health concern.

Drug resistance in *M. tuberculosis* is due primarily to single-nucleotide polymorphisms in genes encoding key mycobacterial enzymes (6). The *rpoB* gene encodes the β-subunit of bacterial RNA polymerase, which is the target of rifampin (12, 41). Mutations in this gene account for over 95% of clinical cases of rifampin resistance (70) and are commonly associated with the presence of MDR TB (27, 65). Although some rifampin-resistant strains demonstrate mild *in vitro* fitness losses compared to wild-type (WT) parental strains, the most common *M. tuberculosis* clinical strains containing the most frequent *rpoB* mutations (e.g., the S531L mu-

tation) tend to exhibit little or no fitness defects, suggesting that certain *M. tuberculosis* isolates are capable of overcoming, at least to some extent, initial fitness deficiencies associated with antibiotic resistance (24, 25). Bergval et al. reported a 2- to 5-fold induction of the stress response gene *dnaE2* (but not *recA*) in four of six *rpoB* mutants of *M. tuberculosis* compared to their wild-type isogenic parent strains using reverse transcription (RT)-PCR (5). However, relatively little is known about *M. tuberculosis* adaptive mechanisms, which may compensate for mutations in *rpoB*. Recently, compensatory mutations in RNA polymerase genes in *rpoB* mutant isolates of *M. tuberculosis* have been identified by comparative genomics (18).

Specific gene upregulation associated with *rpoB* mutation has been observed in numerous model organisms, including *Streptomyces* spp., which are environmental organisms phylogenetically related to *M. tuberculosis* (35, 37, 69). Moreover, upregulation of certain gene clusters via *rpoB* mutation has been used in actino-

mycetes as a way to discover new secondary metabolites, including antibiotics (34). This suggests that *rpoB* mutation may have analogous effects on specific gene upregulation in *M. tuberculosis*. The *M. tuberculosis* genome has an extensive array of polyketide synthase genes (17), which have been shown in other bacteria to be involved in the biosynthesis of secondary metabolites, including rifamycins (28). *rpoB* is an essential gene in *M. tuberculosis*, and clinically relevant *rpoB* mutations occur near the DNA-RNA channel of bacterial RNA polymerase (12, 64). We hypothesized that *rpoB* mutations would lead to altered expression of specific genes/proteins in rifampin-resistant strains. In the current study, we compared the proteomes and metabolomes of paired wild-type and *rpoB* mutant *M. tuberculosis* clinical isolates to identify possible compensatory mechanisms important to drug-resistant isolates of the pathogen. Identification of these pathways may yield new drug targets and diagnostics that can improve treatment of patients infected with rifampin-resistant *M. tuberculosis* isolates.

MATERIALS AND METHODS

***M. tuberculosis* strains.** All *M. tuberculosis* strains were obtained from patients being treated for pulmonary TB. Isolates were sent to National Jewish Hospital, Denver, CO, for confirmation of drug susceptibility data that were initially obtained by the clinical laboratories where the patients were being treated. An *M. tuberculosis* strain susceptible to all drugs tested (rifampin, isoniazid, pyrazinamide, and ethambutol) was obtained from a patient living in Costa Rica prior to initiating antitubercular therapy. Another isolate was later obtained from the same patient after several weeks on treatment and was confirmed to be resistant to rifampin by the agar proportion test (MIC > 1 mg/liter) but susceptible to the other 3 first-line agents. These isolates were a parent-mutant pair by spoligotyping and insertion sequence *6110* (IS*6110*) restriction fragment length polymorphism (RFLP) pattern. Spoligotyping analysis determined that these isolates belong to the Beijing family. Analysis of genomic DNA from these strains revealed an H445D mutation in the *rpoB* gene of the rifampin-resistant isolate. Both isolates also had an A463G mutation in *katG* but were confirmed to be susceptible to isoniazid (MIC < 0.2 mg/liter), and these mutations were considered clinically silent (31, 60). Similarly, an *M. tuberculosis* strain susceptible to all drugs tested (rifampin, isoniazid, pyrazinamide, and ethambutol) was obtained from a patient in San Francisco prior to initiating standard first-line antitubercular therapy. After several weeks on therapy, another isolate was obtained from the same patient and was confirmed to be resistant to rifampin by an agar proportion test (as described above) but susceptible to the other 3 first-line agents. These isolates were also confirmed as paired by spoligotyping and IS*6110* RFLP and were determined to belong to the Haarlem family. Analysis of genomic DNA from these two Haarlem isolates revealed that the rifampin-resistant isolate had an S450L mutation in the *rpoB* gene. Both isolates also had a mutation at position 103 of the *rpoB* gene, and the wild-type strain had an additional mutation at position 108 of *oryR*. The *rpoB* mutations present in the resistant isolates are two of the most common rifampin resistance mutations encountered clinically in adults with TB (70).

For laboratory-based *rpoB* mutant generation used in confirmatory experiments, an exponentially growing culture of the Johns Hopkins University wild-type laboratory reference strain *M. tuberculosis* CDC1551 (1) was inoculated onto 7H10 agar containing 1 μg/ml rifampin and incubated at 37°C for 21 days. Individual colonies were inoculated separately in Middlebrook 7H9 broth containing 1 μg/ml rifampin and grown at 37°C to an optical density at 600 nm (OD$_{600}$) of ~1.0. Genomic DNA was purified from each culture, and the *rpoB* gene was amplified using primers 5′-AATATCTGGTCCGCTTGCAC-3′ and 5′-ACACGATCTCGTCGCT AACC-3′ and sequenced. Based on the sequencing results, a mutant con-taining a substitution of G for C at bp 1351 in the *rpoB* gene (yielding the RpoB S450L mutation) was selected for further study.

Culture conditions. For proteomics studies, a glycerol stock of each strain was plated in Middlebrook 7H11 (Difco) supplemented with oleic acid-albumin-dextrose-catalase (OADC). After incubation for 2 weeks at 37°C, colonies were inoculated in 100 ml of Middlebrook 7H9 (Difco) supplemented with OADC and 0.05% Tween. The mycobacteria were further cultured at 37°C with agitation for 2 weeks and then washed twice with sterile phosphate-buffered saline (PBS) (Invitrogen) and inoculated in 1 liter of GAS (glycerol, alanine, salts) medium (68), a traditional *Mycobacterium* sp. medium used to process cells and spent filtrate for downstream proteomics applications (4, 55, 63). The cultures were then incubated at 37°C with agitation for 4 weeks. All cultures were prepared in triplicate for proteomics analyses. For metabolomics studies, a glycerol stock of each strain was plated in Middlebrook 7H11 (Difco) supplemented with OADC. The cultures were incubated at 37°C for 4 weeks. Five replicates per strain were prepared for metabolomics studies.

CFP. Proteomics data were obtained within specific cellular fractions, consisting of culture filtrate (CFP), membrane-associated (MEM), cell wall (CW), and cytoplasm (CYT) proteins. CFP was purified as described elsewhere (55). Briefly, each culture was filtered using a 0.2-μm Whatman zap-cap filter (GE Healthcare, Piscataway, NJ). The secreted proteins were recovered from the culture filtrate as follows: 1 liter culture filtrates was concentrated to approximately 25-ml volume using a 10-kDa molecular mass cutoff membrane (Millipore). Then, the filtrate was further concentrated to approximately 300 μl using an Amicon Ultracell-15 with a 10,000 molecular weight cutoff by centrifugation at 3,000 rpm at 4°C. The purified proteins were subjected to buffer exchange using 15 ml of 10 mM ammonium bicarbonate three times in the same filter unit. Protein quantification was performed by the bicinchoninic acid (BCA) assay (Pierce).

Subcellular fractions. Cells were pelleted by centrifugation at 3,000 rpm and washed twice with 10 ml of sterile PBS (Invitrogen). The harvested cells were inactivated with 2.4 Mrad of cesium gamma irradiation for 24 h, and death was confirmed by alamarBlue assay (Invitrogen). The cells were resuspended in 10 ml of breaking buffer (1 mM EDTA-PBS supplemented with one tablet of protease inhibitor [Roche Diagnostics] per 50 ml of buffer, 60 μl of DNase [1 mg/ml], and 60 μl of RNase [1 mg/ml]) and broken by sonication on a 50% duty cycle (12 times; 60 s with intervals of 90 s on ice). After sonication, breaking buffer was added to a final volume of 40 ml, and unbroken cells were removed by centrifugation at 3,000 rpm for 5 min at 4°C. The supernatant was further centrifuged for 1 h at 27,000 × g at 4°C to separate the cell wall pellet from the cytosol and membrane fractions (supernatant). The cell wall pellet was resuspended in 10 mM ammonium bicarbonate and stored at −80°C. Finally, membrane proteins were harvested by ultracentrifugation at 100,000 × g for 8 h (2 times for 4 h each time). The cytosol fraction (supernatant) was concentrated by centrifugation using Amicon Ultra-15 centrifugal filter units with a 10-kDa molecular mass cutoff. Buffer exchange using 15 ml of 10 mM ammonium bicarbonate was performed three times using the same filter unit. The membrane fraction was resuspended in 10 mM ammonium bicarbonate and stored at −20°C. All subcellular fractions were quantified using the BCA assay (Pierce).

In-solution protein digestion. Fifty micrograms of the CFP, MEM, and CYT fractions was precipitated with acetone following standard protocols. The protein pellets were resuspended in 15 μl of 8 M urea, followed by addition of 20 μl of 0.2% ProteaseMax Surfactant (Promega) in 50 mM ammonium bicarbonate. After vortexing for 5 min, 58.5 μl of 50 mM ammonium bicarbonate was added to each sample. Proteins were reduced after incubation at 50°C for 20 min with 5 mM dithiothreitol (DTT). Alkylation was performed with 15 mM iodoacetamide, followed by incubation at room temperature for 15 min in the dark. Samples were digested for 3 h at 37°C with 1 μl of 1% ProteaseMax Surfactant (Promega) in 50 mM ammonium bicarbonate and 1.8 μg of trypsin. Reactions were stopped with 0.5% trifluoroacetic acid (TFA). All samples were desalted with Pierce PepClean C$_{18}$ spin columns according to the manufacturer's

protocol and eluted with 70% acetonitrile (ACN), 0.1% formic acid (FA). Samples were dried in a SpeedVac and resuspended in 5% ACN, 0.1% FA prior to mass spectrometry analysis. Biological replicates within each cellular fraction were randomized and injected in triplicate. Mass spectrometry analysis was performed at the Proteomics and Metabolomics Facility, Colorado State University, Pueblo, CO.

CW proteins were subjected to a delipidation protocol before digestion as follows. Ten micrograms of lysozyme was added to 1 mg of CW proteins and incubated for 30 min at 37°C. Samples were dried in a SpeedVac and resuspended in 7 ml of chloroform-methanol (2:1 [vol/vol]), followed by incubation at room temperature for 1 h and centrifugation at 3,000 rpm for 30 min at 4°C. The pelleted proteins were dried and resuspended in 7 ml of chloroform-methanol-water (10:10:3), followed by incubation with agitation at room temperature for 1 h and centrifugation at 3,000 rpm for 2 h at 4°C. Finally, the pelleted proteins were precipitated with 2 ml of cold acetone and incubated overnight at −20°C. After centrifugation at 13,000 rpm for 30 min, the protein pellet was resuspended in 10 mM ammonium bicarbonate, and quantification was performed using the BCA assay (Pierce). Fifty micrograms of sample was subjected to trypsin digestion as described above.

LC–MS-MS for proteomics studies. All samples were randomized and analyzed in triplicate by liquid chromatography coupled with tandem mass spectrometry (LC–MS-MS). Briefly, peptides were purified and concentrated using an on-line enrichment column (Agilent Zorbax C_{18}; 5 μm; 5 by 0.3 mm). Subsequent chromatographic separation was performed on a reverse-phase nanospray column (Agilent 1100 nanoHPLC; Zorbax C_{18}; 5 μm; 75-μm inside diameter [ID] by 150-mm column) using a 60-min linear gradient from 25% to 55% buffer B (90% ACN, 0.1% formic acid) at a flow rate of 300 nl/min. Peptides are eluted directly into the mass spectrometer (Thermo Scientific Linear Trap Quadrupole [LTQ] linear ion trap), and spectra are collected over an *m/z* range of 200 to 2,000 Da using a dynamic-exclusion limit of 2 MS-MS spectra of a given peptide mass for 30 s (exclusion duration, 90 s). Compound lists of the resulting spectra were generated using Bioworks 3.2 software (Thermo Scientific) with an intensity threshold of 5,000 and 1 scan/group.

Spectra were subjected to interrogation against the *M. tuberculosis* genome (including the reverse strand) (GenBank accession number AL123456, R9; 7,982 entries) using SORCERER (Sage-N Research, version 2.0) and SEQUEST (Thermo Fisher Scientific, release 27, revision 12). All searches were performed assuming trypsin digestion, 4 missed cleavages, a fragment ion mass tolerance of 1.00 Da, and a parent ion tolerance of 1.5 Da. Carbamidomethyl (C) and oxidation (M) were specified as variable modifications. Analyses (per subcellular fraction) were compiled in Scaffold (version 3.00.04; Proteome Software Inc., Portland, OR) in order to validate MS-MS-based peptide and protein identification. Search results for triplicate injections of each biological replicate were summed together upon compilation within the Scaffold software. In addition, the X! Tandem database search algorithm (version 2007.01.01.2; The Global Proteome Machine [http://www.thegpm.org]) was used to verify and complement the peptide identifications from Sequest. Peptide identifications were filtered by database search engine thresholds, so that Sequest identifications required deltaCn scores greater than 0.10 and XCorr scores greater than 1.0, 2.0, 3.0, and 3.0 for singly, doubly, triply, and quadruply charged peptides, respectively. X! Tandem identifications required −Log(Expect Scores) scores greater than 2.0. Protein identifications were accepted if they could be established at greater than 99.0% probability (Protein Prophet algorithm) and contained at least 1 unique peptide (45). False-discovery rates (FDR) were calculated automatically by Scaffold (version 3.0) using the decoy database and reverse hits and the empirical method previously reported by Kall et al. (42). Analysis of each data set using these parameters resulted in FDR of 0.2% at the protein level and less than 5.3% at the peptide level. After statistical analysis, different proteins that were identified by only one unique peptide were subjected to manual spectral validation using the following criteria: (i) a minimum of 80% coverage of theoretical y or b ions (at least 5 in consecutive order), (ii)

absence of prominent unassigned peaks at greater than 10% of the maximum intensity, and (iii) indicative residue-specific fragmentation, such as intense ions proximal (N-terminal) to proline and immediately distal (C-terminal) to aspartate and glutamate. The data, exported as Mascot generic files and containing all MS-MS spectra, are available in the PRoteomics IDEntifications database for review (74).

Proteomic data analysis. Each subcellular fraction data set was subjected to spectral-count analysis using Scaffold (version 3.00.04; Proteome Software Inc., Portland, OR). Technical replicates for each biological replicate were summed within the Scaffold software, and each subcellular fraction data set was analyzed independently. Prior to all analyses of differential protein detection, spectral counts were normalized against the total signal (per biological replicate) as described previously (14). Using spectral counts, differential protein detection was assessed in multiple ways. First, after normalization, the data were log transformed, and a linear-model analysis of variance (ANOVA) comparing spectral counts for each protein within subcellular fractions for each isogenic pair was applied to identify proteins that were differentially abundant between susceptible and resistant isolates (*P* value < 0.05). Comparison of spectral counts was performed using DanteR (version 1.0.1.1; Pacific Northwest National Laboratory [http://omics.pnl.gov]). The reproducibility of biological replicates was assessed by visual interpretation of each data set using box plots and three-dimensional (3D) scatter plots generated on DanteR.

In addition, to ascertain global differences in protein detection between *rpoB* mutant and wild-type isolates, the mean spectral counts in the cell-associated fractions (CW, MEM, and CYT) were added to produce a summary spectral count for each protein. CFP was not included in the summary spectral count, given our interest in measuring differences in overall protein abundance and not secretion. This summary cell-associated spectral count was then used to calculate the fold change in detection for each protein by dividing the mean spectral count in an *rpoB* mutant by the mean spectral count in the paired wild-type parent isolate. The summary cell-associated spectral counts were also used to calculate the spectral index (SpI), which is a robust statistical measure of differential protein abundance useful in shotgun proteomics experiments (23). We then used the SpI, which ranges from −1 to +1, to rank order the proteins by the degree of increased detection in mutants. SpI values at or near 0 indicate that the relative peptide abundances are approximately the same in the rifampin-resistant and rifampin-susceptible cultures, whereas positive or negative values indicate enrichment in the rifampin-resistant or rifampin-susceptible cultures, respectively (23). With this ranking, we then applied gene set enrichment analysis (GSEA) at the functional class level to identify significantly upregulated gene sets in the resistant strains (67). Because *rpoB* mutation appears to significantly upregulate genes specifically involved in biosynthesis of natural product/secondary metabolites in other organisms (13, 34, 35, 37), we also used an automated approach to search the *M. tuberculosis* genome for gene clusters potentially associated with natural product biosynthesis (NP.searcher) (http://dna.sherman.lsi.umich.edu/; 49) and compared the expression of these gene clusters by mutants and wild-type *M. tuberculosis* using GSEA.

Macrophage studies. The murine macrophage J774A.1 cell line was cultured in RPMI medium supplemented with 0.2 mM L-glutamine (Invitrogen) and 10% heat-inactivated fetal bovine serum (FBS) (Sigma) in a humidified 37°C, 5% CO_2 incubator. After growth to a confluent monolayer, the cells were harvested using a sterile rubber scraper, and a single-cell suspension was prepared and cultured in a 75-cm^2 cell culture flask (Costar). A total of 10^3 cells were activated by addition of 50 ng/ml gamma interferon (IFN-γ) (Roche) overnight and 200 ng/ml lipopolysaccharide (LPS) (from *Escherichia coli* 026:B6; <5% protein [Lowry]; Sigma) for 3 h prior to infection. After removal of the medium, the cells were incubated for 3 h with either wild-type *M. tuberculosis* or the *rpoB* mutant at a multiplicity of infection (MOI) of 1:1. The macrophages were then treated with 200 ng/ml streptomycin, washed three times with RPMI, and cultured in medium as described above. For bacterial enumeration for com-

parison of the growth rates of the mutant and WT isolates, the cells were lysed with Triton X-100 at predetermined time points, and the lysate was serially diluted and plated on 7H10 agar and incubated at 37°C for 28 days, as previously described (71). For mycobacterial gene expression studies, intracellular bacteria were recovered at 72 h after infection by centrifugation at 3,200 rpm for 5 min, and the bacterial pellet was resuspended in TRIzol reagent (Invitrogen).

M. tuberculosis gene expression studies. Macrophage and mycobacterial membranes were disrupted using 0.1-mm zirconia/silica beads in a bead beater, and RNA was recovered by centrifugation, chloroform extraction, and isopropyl alcohol precipitation, as previously described (43, 44). Prior to reverse transcription, control and mutant RNAs (10 ng) were treated with RNase-free DNase (Invitrogen) and subjected to 36 cycles of PCR to ensure that all DNA had been removed, as assessed by ethidium bromide-stained agarose gel analysis. Fluorescently labeled cDNA was generated using gene-specific primers (see Table S1 in the supplemental material) and Superscript III (Invitrogen), as previously described (71). cDNA corresponding to each transcript was subjected to 40 cycles of PCR for quantification using the primers listed in Table S2 in the supplemental material and an iCycler 5.0 (Bio-Rad). The cycle threshold (C_T) value obtained for each gene of interest (GOI) was normalized with that of *sigA*, a housekeeping gene (HKG) with constant expression under different experimental conditions (53), in order to obtain the normalized C_T [$nC_T = $ (GOI C_T) − (HKG C_T)]. The change in the normalized C_T (ΔnC_T) for each gene was calculated using the following formula: $\Delta nC_T = $ C(nC_T) − S(nC_T), where C represents the wild-type (control) strain and S represents the *rpoB* mutant strain. The fold regulation of individual genes was calculated using the following formula: $2^{-\Delta nCT}$. The data are representative of three biological replicates, and the experiments were repeated twice.

Extraction of M. tuberculosis metabolites. Mycobacteria were scraped at 4 weeks of culture and transferred to a glass tube; 10 ml of chloroform was added to each sample and then incubated at room temperature in agitation for 4 h. The bacteria were pelleted at 3,000 rpm for 30 min at 4°C, and the supernatant corresponding to the chloroform fraction was dried in a nitrogen bath and stored at −20°C. The pelleted bacteria were dried under nitrogen and then resuspended in 15 ml of methanol. Samples were incubated at 37°C overnight with agitation and then centrifuged at 3,000 rpm for 1 h at 4°C. Supernatant corresponding to the methanol fraction was dried under nitrogen and then stored at −20°C. Prior to mass spectrometry analysis, the chloroform and methanol fractions were resuspended in 1 ml of the corresponding solvent.

LC-MS for metabolomics. (i) Methanol fractions. One microliter of the sample was injected into a Waters Acquity Ultra Performance Liquid Chromatography (UPLC) system equipped with a Waters Acquity UPLC T3 column (1.8 μm; 1.0 by 100 mm). Separation was achieved using a gradient from solvent A (95% water, 5% methanol, 0.1% FA) to solvent B (95% methanol, 5% water, 0.1% FA) as follows: 100% A held for 1 min, 100% B in 16 min, 100% B held for 3 min, 100% A in 0.1 min, and reequilibration for 5.9 min (total run time, 26 min/sample).

(ii) Chloroform fractions. One microliter of the sample was injected on a Waters Acquity UPLC system equipped with a Waters Acquity UPLC C$_8$ column (1.8 μM; 1.0 by 100 mm). Separation was achieved using a gradient from solvent A (89% water, 5% ACN, 5% isopropanol, 1% 500 mM ammonium acetate) to solvent B (49.5% ACN, 49.5% isopropanol, 1% 500 mM ammonium formate) as follows: 100% A held for 0.1 min, 40% B in 0.9 min, 100% B in 10 min, 100% B held for 3 min, 100% A in 0.1 min, and reequilibration for 5.9 min (total run time, 20 min/sample). MS-MS spectra of precursor ions 797.7 and 823.2 were collected using a Waters UPLC coupled to a Waters Xevo G2 quadrupole-time-of-flight (Q-TOF) MS. The LC conditions were the same as those listed above, and the MS-MS collision energy was ramped from 15 to 30 V to induce fragmentation.

For both fractions, the flow rate was maintained at 140 μl/min for the duration of the run, the column was held at 50°C, and samples were held at 5°C. The column eluate was infused into a Waters Q-TOF Micro MS fitted with an electrospray source. Data were collected in positive ion mode, scanning from 50 to 1,200 (methanol fraction) or 50 to 1,800 (chloroform fraction) at a rate of 0.9 s per scan with 0.1-s interscan delay. Calibration was performed prior to sample analysis via infusion of sodium formate solution, with mass accuracy within 5 ppm. During analysis, the capillary voltage was held at 2,200 V, the source temperature at 130°C, the desolvation temperature at 300°C, the desolvation gas flow rate at 400 liters/h N$_2$ (gas), and the quadrupole at a collision energy of 7 V. The MS-MS spectra of precursor ions 797.7 and 823.2 were collected using a Waters UPLC coupled with a Waters Xevo G2 Q-TOF MS. The LC conditions were the same as those listed above, and the MS-MS collision energy was ramped from 15 to 30 V to induce fragmentation.

(iii) Metabolomics data analysis. Raw data files were converted to .cdf format, and feature detection and alignment were performed using XCMS in the program R. Raw peak areas were normalized to the total ion signal in R, and the normalized data set was subjected to PCA in R using the pcaMethods package. Consistent with our focus on gene upregulation as a compensatory response to *rpoB* mutation, statistical analysis to determine peaks/features that were significantly more abundant in resistant strains was performed in DanteR, as described for proteomics above. Differential peaks (ANOVA; P value < 0.05) were grouped by retention time and then manually validated using MassLynx (Waters Corporation). Peaks with the same retention time and peak shape were considered to belong to the same compound. The retention time and the inferred molecular weight of each differential peak was used to interrogate public databases, including METLIN (http://metlin.scripps.edu) (66), KEGG (http://www.genome.jp /kegg/), LipidMaps (http://www.lipidmaps.org), and MassBank (http: //www.massbank.jp) (33). Given the proteomics and metabolomics results, a phthiocerol dimycocerosate (PDIM) standard was subjected to tandem mass spectrometry analysis to gain insight into the structure of the *m/z* 797.74 ion.

TLC. Two hundred micrograms of lipid fractions was analyzed by thin-layer chromatography (TLC), along with a PDIM standard (10 μg), using 98:2 (vol/vol) petroleum ether-ethyl acetate three times. Lipids were visualized with CuSO$_4$ charring.

RESULTS

Proteomic analysis of *rpoB* mutant strains of *M. tuberculosis*. To compare the proteomes of the Beijing and Haarlem strains of *rpoB* mutant, rifampin-resistant *M. tuberculosis* to those of their wild-type progenitor isolates, proteins from four cellular fractions were extracted from late-log-phase broth cultures. By separating the sample into less complex parts, such as subcellular fractions, protein identification using shotgun proteomic analysis is greatly increased (22, 36). In addition, because of the insoluble nature of cell wall proteins, this fraction is subjected to additional preparation prior to mass spectrometry analysis to increase solubility and the number of identified proteins. After digestion into tryptic peptides, each fraction was analyzed independently in triplicate by LC–MS-MS. The spectra were searched against the *M. tuberculosis* genome, and the total number of unique peptides identified in each cellular fraction of each biological replicate by strain type is shown in Table S3 in the supplemental material. Totals of 452, 1,075, 807, and 735 proteins were confidently identified in the CFP, CW, MEM, and CYT fractions, respectively, of the Haarlem isolates, and 455, 1,072, 760, and 704 proteins were confidently identified in the CFP, CW, MEM, and CYT fractions, respectively, of the Beijing isolates.

Spectral counts for each biological replicate were normalized against the total signal as described previously (14). After normalization and log transformation of the data, a linear-model

TABLE 1 Mean spectral counts and functional classes of proteins detected at statistically significantly higher spectral counts in specific cellular fractions of both *rpoB* mutant versus wild-type parent strains of *M. tuberculosis*

Protein name (gene)	Rv no.	Fraction	Functional class	Spectral count[a]					
				Haarlem			Beijing		
				rpoB	WT	*P* value	*rpoB*	WT	*P* value
Succinic semialdehyde dehydrogenase (*gabD1*)	Rv0234c	CYT	Intermediary metabolism and respiration	29	21	0.003	24	15	0.002
Hypothetical protein Rv1056	Rv1056	CFP	Conserved hypothetical	32	11	0.029	41	17	0.037
Putative integration host factor MIHF (*mihF*)[b]	Rv1388	CFP	Information pathways	5.35[b]	0	0.022	4.61	0	0.009
Probable acyl-CoA dehydrogenase FADE31 (*fadE31*)	Rv3562	CFP	Lipid metabolism	2.34	0	0.004	2.05	0	0.002
Polynucleotide phosphorylase/polyadenylase (*gpsI*)	Rv2783c	MEM	Information pathways	74.78	44.32	0.038	95.96	54.98	0.003
Hypothetical protein Rv3038c	Rv3038c	MEM	Conserved hypothetical	10.87	1.37	0.014	3.89	0.66	0.045
Hypothetical protein Rv3661[b]	Rv3661	MEM	Conserved hypothetical	9.43	0.73	0.012	7.29	2.51[b]	0.007
Phenolpthiocerol synthesis type I polyketide synthase (*ppsC*)	Rv2933	CW	Lipid metabolism	16.32	4.98	0.001	41.74	3.66	0.029
Phenolpthiocerol synthesis type I polyketide synthase (*ppsE*)	Rv2935	CW	Lipid metabolism	41.69	19.75	0.049	65.64	32.15	0.041
Probable daunorubicin-DIM-transport ATP-binding protein ABC transporter (*drrA*)	Rv2936	CW	Cell wall and cell processes	3.83	0	0.012	6.55	1.41	0.034

[a] The spectral counts are the means of 3 biological replicates for each isolate. The numbers correspond to normalized spectral counts.
[b] Protein identified by only 1 unique peptide in all biological replicates. See Fig. S1a to f in the supplemental material for spectra of these two proteins.

ANOVA comparing spectral counts for each protein within subcellular fractions for each isogenic pair was applied to identify proteins that were differentially abundant between susceptible and resistant isolates (P value < 0.05). Thirty-two, 44, 21, and 27 proteins with significantly higher spectral counts ($P < 0.05$) than the wild-type isolate were identified in the CFP, CW, MEM, and CYT fractions, respectively, of the Haarlem *rpoB* mutant. Similarly, there were 45, 44, 43, and 31 proteins with significantly higher spectral counts detected in the CFP, CW, MEM, and CYT fractions, respectively, of the Beijing *rpoB* mutant isolate than in those of its wild-type progenitor isolate. A comparison of both *rpoB* mutants with their respective wild-type rifampin-susceptible parent revealed 10 proteins with statistically significantly ($P < 0.05$) higher normalized spectral counts (Table 1). All of the products identified at significantly higher spectral counts in the cell wall fractions of both *rpoB* mutant rifampin-resistant strains represented proteins that are transcriptionally coupled on a 50-kb region involved in the biosynthesis of PDIM in *M. tuberculosis* (10, 72), including two type I polyketide synthase genes (Rv2933/*ppsC* and Rv2935/*ppsE*) and a probable daunorubicin-dimycoserosate (DIM) transport protein (Rv2936/*drrA*). Other proteins identified in cellular fractions other than the cell wall included a succinate semialdehyde dehydrogenase (Rv0234c), a putative integration host factor (Rv1388/*mihF*), a probable acyl-coenzyme A (CoA) dehydrogenase (Rv3562/*fadE31*) involved in lipid degradation, and a polynucleotide phosphorylase/polyadenylase (Rv2783c/*gpsI*) involved in mRNA degradation. The final three products identified (Rv1056, Rv3038c, and Rv3661) are conserved hypothetical proteins with unknown functions (Table 1). We specifically examined spectral counts of *recA* and *dnaE2* based on a previous study using quantitative RT (qRT)-PCR (5) but did not find increased spectral counts for the corresponding proteins (data not shown). Table S4 in the supplemental material shows the number of proteins detected in the *rpoB* mutant Haarlem and Beijing isolates at summary (combined CW, MEM, and CYT) spectral counts at least 2-fold higher than those of the

wild-type isolates, as well as the number of proteins detected in the mutant isolates alone (where the fold change is set arbitrarily to 100). There were 25 proteins detected in neither wild-type isolate and in both *rpoB* mutants (see Table S4 in the supplemental material). Five of these proteins were detected in at least 2 replicates in both *rpoB* mutants, as shown in Table S5 in the supplemental material. Table S5 lists the Rv numbers, spectral counts, fold changes, replicate raw data, and *P* values for the comparison of the two strains for the 90 cell-associated proteins detected at >2-fold-higher levels in both *rpoB* mutant isolates than in the wild type, including proteins detected only in the mutant strains. Of the 10 proteins identified at statistically significantly higher counts in specific cellular fractions of both *rpoB* mutants (Table 1), 3 also had summary cell-associated (e.g., combined spectral counts of all fractions except CFP) spectral counts at least 2-fold higher in both mutants than in the wild-type isolates, and of these, 2 involved the PDIM biosynthetic locus (*ppsC* and *drrA*). The increased detection levels in the *rpoB* mutant Haarlem and Beijing isolates of *ppsC* and *drrA* were 3.6 and 10.2, and 100 (detected in the mutant but not the wild type) and 4.7, respectively. The fold change values for *ppsE* were 3.07 and 1.97 for the Haarlem and Beijing strains, respectively.

Gene set enrichment analysis of proteins upregulated in both *rpoB* mutants. The distributions of functional classes among genes upregulated ≥2-fold in both *rpoB* mutants versus genes not upregulated in both mutants were not statistically significantly different when the proportions of genes in each functional categorization of gene products (COG) class were compared (chi-square tests, all $P > 0.05$). Among the four gene loci identified as possibly involved in natural product biosynthesis in *M. tuberculosis* by NP.searcher, the polyketide synthase gene cluster *ppsA-ppsE* and *drrA* was significantly upregulated in both *rpoB* mutants (Fig. 1).

Selected expression of genes in the PDIM biosynthetic locus in the Beijing *rpoB* mutant *M. tuberculosis* during active infection of murine macrophages. In order to determine if increased
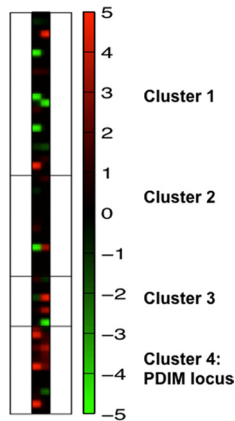
FIG 1 Heat map of protein detection in *rpoB* mutant versus wild-type strains as determined by summary cell-associated spectral counts in 4 gene clusters identified as possibly involved in natural product biosynthesis by NP.searcher. The PDIM biosynthetic locus is cluster 4. Cluster 1, Rv0993-Rv1017c; cluster 2, Rv1536-Rv1551; cluster 3, Rv1661-Rv1668c; cluster 4, Rv2930-Rv2943. Genes are shown in increasing order of Rv number from top to bottom. The column on the left corresponds to the Haarlem strains, while the one on the right corresponds to the Beijing strains.

expression of proteins involved in PDIM biosynthesis correlated with increased transcription of the corresponding genes, qRT-PCR was performed. Consistent with the proteomic analysis, the *ppsA* gene was found to be upregulated >2-fold in the Beijing *rpoB* mutant relative to the parental strain (Fig. 2A). Next, using qRT-PCR, we sought to determine the effect of *rpoB* mutation on the

expression levels of selected PDIM biosynthesis genes during *M. tuberculosis* infection of activated murine macrophages. The genes *ppsA*, *ppsC*, and *ppsE* were each found to have >10-fold-increased expression in the *rpoB* mutant relative to the rifampin-sensitive parent strain, while expression of the control gene Rv0496 was not different between the two strains (Fig. 2B). A comparison of up-regulation in Fig. 2A and B indicates that the upregulation was more striking in activated macrophages than in nutrient-rich medium. Consistent with the proteomic data, Rv0799c, which encodes a conserved hypothetical protein, was also found to be mildly upregulated in the *rpoB* mutant relative to the parent strain in activated murine macrophages. The *rpoB* mutation did not appear to confer a fitness cost, as the *rpoB* mutant and the WT parent strain showed nearly equivalent growth rates and survival in activated macrophages (Fig. 2C). Finally, in order to confirm that the gene expression profile observed in the *rpoB* mutant was attributable to the RpoB S450L mutation in the *rpoB* gene, we experimentally generated a mutant strain containing the RpoB S450L mutation in the background of the laboratory strain *M. tuberculosis* CDC1551. The genes *ppsA*, *ppsB*, *ppsC*, and Rv0799c were each upregulated in this *rpoB* S450L mutant relative to the isogenic CDC1551 WT strain during logarithmic growth in nutrient-rich broth (Fig. 2D).

Metabolomics analysis. In addition to the proteomics experiments described above, metabolomics analyses were performed in order to determine if *rpoB* mutations also might lead to changes in the *M. tuberculosis* metabolome. Because of the great complexity of the sample, two sequential extractions were performed to separate cell wall-associated lipids and other nonpolar metabolites
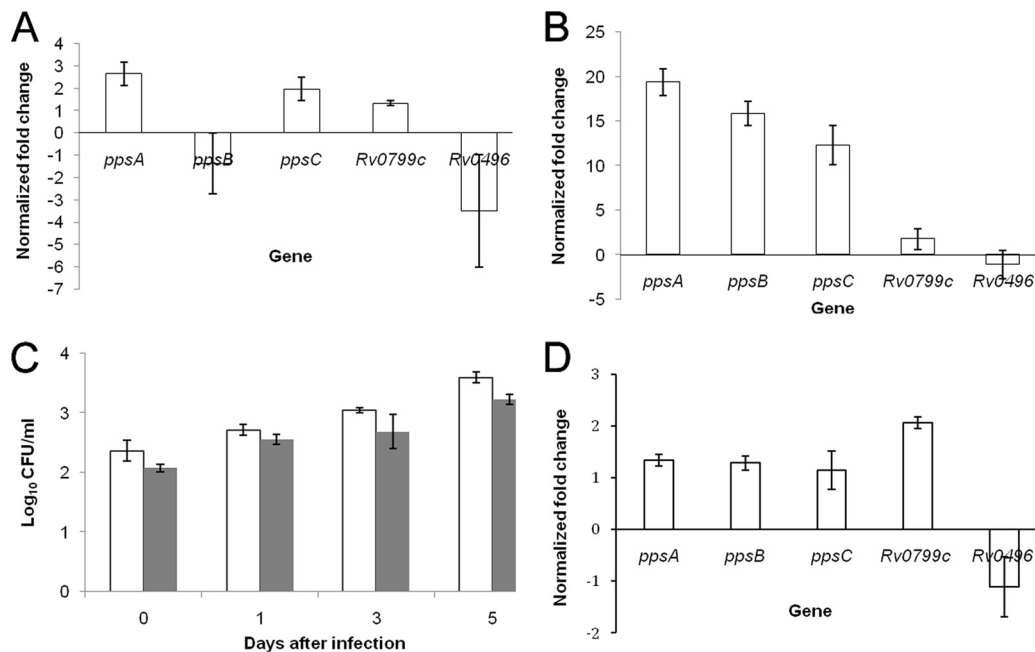

FIG 2 Effects of *rpoB* S450L mutation on *M. tuberculosis* gene expression and fitness. (A) Expression of the PDIM biosynthesis locus in the *rpoB* mutant Beijing strain relative to the rifampin-sensitive wild-type parent strain during logarithmic growth in nutrient-rich broth, as measured by RT-PCR. (B) Gene expression of the same strains after 72 h of infection in activated murine macrophages. (C) Growth and survival of the *rpoB* mutant (gray) relative to the Beijing wild-type parent strain (white) in activated murine macrophages. (D) RT-PCR analysis of gene expression in a laboratory-generated RpoB S450L mutant relative to the isogenic CDC1551 wild-type strain during logarithmic growth in nutrient-rich broth. The C_T obtained for each gene of interest was normalized with that of the housekeeping gene *sigA*. Fold regulation of individual genes was calculated using the following formula: $2^{-[C(CT) - S(CT)]}$, where C represents the wild-type (control) strain and S represents the *rpoB* mutant strain. The error bars indicate standard deviations.

from more polar metabolites. This analysis revealed 99 molecular features in the chloroform fraction that were significantly more abundant ($P < 0.05$) in both rifampin-resistant *M. tuberculosis* strains than in their susceptible counterparts (see Table S6 in the supplemental material). A search performed against the Lipid-Maps database suggested that several of these significant features correspond to diacylglycerol phosphocholines (Table 2). Since the proteomics and GSEA findings suggested that the polyketide synthase genes involved in phenolpthiocerol biosynthesis are upregulated in the *rpoB* mutant isolates of *M. tuberculosis*, we compared the chloroform extract to a positive authentic PDIM standard that was obtained from *M. tuberculosis* H37Rv and analyzed by LC-MS using identical parameters. The PDIM standard was obtained through the Tuberculosis Vaccine Testing and Research Material Contract (TVTRMC). The 797.7 *m/z* and 823.2 *m/z* signals, observed to increase in the resistant strains relative to their respective parent strains (Fig. 3 and Table 2), were also found in an authentic PDIM standard. When MS-MS analysis was performed on the 797.7 *m/z* ion, a fragment of 523.47 *m/z* and neutral loss of 274.27 were observed (data not shown). The difference of 2 Da from the expected 525.5 *m/z* of phthiocerol (40) suggests desaturation by loss of the methyl group and therefore most likely corresponds to phthiodiolone. These data are consistent with accumulation of PDIM precursors in the rifampin-resistant isolates, perhaps due to elevated levels of polyketide synthase-related proteins.

Eighty-seven molecular features from the methanol fraction were significantly more abundant ($P < 0.05$) in both resistant strains than in their susceptible counterparts (see Table S6 in the supplemental material). A large portion of these molecular features were observed in two clusters at a retention time of 16.9 min, suggesting that they may be derived from a common parent compound (Table 2). Each cluster of peaks was searched against the MassBank spectral database, and both returned matches to hexose-*N*-acetyl-hexosamine-fucose-*N*-acetyl-hexosamine (Table 2). To determine if this compound originated from peptidoglycan (PG), an *M. tuberculosis* petidoglycan standard, obtained through the TVTRMC, was analyzed by LC-MS under identical conditions. On comparison, the standard peptidoglycan spectrum did not correlate with the molecular features observed in the methanol sample fraction. However, this was not entirely unexpected, given the extensive cross-linking in mature PG and the stability of the mature product. An analysis of the literature for mass spectra of partially hydrolyzed PG demonstrated reports of PG *N*-acetylmuramic acid (MurNac) tetra- and pentapeptides and MurNac of *M. tuberculosis* PG that do match the molecular features observed in the spectra from our methanol sample fractions. Specifically, the molecular features at 808.6 *m/z* (790.6 *m/z* minus water), 736.6 *m/z* (718.6 *m/z* minus water), and 531.5 *m/z* correspond to these three PG derivatives (48, 52). An examination of the gene cluster associated with peptidoglycan biosynthesis in *M. tuberculosis* (Rv2158c-2152c) did not, however, reveal significantly increased spectral counts in the *rpoB* mutant isolates using GSEA. A previously reported scoring system of 1 to 4 (1, high; 4, low) was used to determine the level of confidence in metabolite identification (http://www.metabolomicssociety.org/).

DISCUSSION

We hypothesized that *rpoB* mutation would lead to upregulation of *M. tuberculosis* genes involved in secondary metabolism, given known relationships between *rpoB* mutation and upregulation of

genes involved in natural product biosynthesis in other organisms (34, 35, 37). This study, which is the first to comprehensively compare the proteomes and metabolomes of *rpoB* mutant rifampin-resistant *M. tuberculosis* with those of their paired wild-type rifampin-susceptible parent strains, supports this hypothesis by demonstrating that several genes, particularly those involved in the biosynthesis of cell wall lipids, including PDIM, are upregulated in *rpoB* mutants, both in broth culture and, in particular, when grown in murine macrophages. Using the program NP.searcher, we found 4 gene loci possibly related to natural product biosynthesis in *M. tuberculosis*, and the GSEA indicated that of these four, the proteins encoded by *ppsA-ppsE* and *drrA* were more abundant in the cell walls of both *rpoB* mutants than in those of their wild-type parent strains. Furthermore, *in situ* overexpression of several *pps* genes was confirmed using a CDC1551 strain, as well as a macrophage model for the Beijing isolate, indicating that the changes in expression of *ppsA-ppsE* are unlikely to be due to inherent characteristics of the two clinical strains used or the *in vitro* culture system. Our study is different from previous studies demonstrating that exposure to rifampin induces several changes in rifampin-resistant *M. tuberculosis* gene expression, including marked upregulation of drug efflux pump-related genes (30, 51). Specifically, in this study, the impacts of *rpoB* mutations on the proteomes and metabolomes of rifampin-resistant and -susceptible strains were studied in the absence of rifampin in order to determine protein and metabolite abundance changes that are associated with *rpoB* mutations independent of drug exposure.

Proteins encoded by *ppsA-ppsE* are involved in PDIM biosynthesis, and the corresponding genes are grouped on a 50-kb fragment of the *M. tuberculosis* chromosome (10). Although we did not find evidence of higher levels of intact PDIM in the Haarlem *rpoB* mutant, levels of PDIM in the Beijing *rpoB* mutant isolate appear to be elevated compared to its isogenic strain, as evaluated by TLC (see Fig. S1 in the supplemental material). However, metabolites with the same spectra as PDIM precursors were detected at higher levels in both *rpoB* mutant isolates compared to their wild-type progenitor isolates. While we evaluated only two strains, the finding of similar changes in protein abundance in a Beijing and a Haarlem strain of *M. tuberculosis* with different *rpoB* mutations grown in the absence of drug exposure suggests that *rpoB* mutation and rifampin resistance in *M. tuberculosis* may lead to a pattern of differential protein and metabolite abundance that is conserved across both mutations and strains, but the extent of this effect may be related to the genetic background of the isolates.

PDIM is a long-chain β-diol (phthiocerol) esterified with two branched-chain mycocerosic acids located in the outer mycobacterial cell wall that has been implicated in *M. tuberculosis* virulence (11, 19, 59). The genes *ppsA-ppsE* (Rv2931-Rv2935) encode a type I modular polyketide synthase responsible for biosynthesis of the phtiocerol backbone of PDIM, with PpsA-PpsC sequentially loading ketide units onto long-chain fatty acids and PpsD and PpsE subsequently extending the phthiocerol further by adding a 4-methyl branch and malonyl- or methylmalonyl-CoA, respectively (3, 72). The genes *drrA-drrC* (Rv2936-Rv2938) are located adjacent to *ppsE* (Rv2935) and are thought to encode proteins involved in the transport and localization of PDIM across the cell membrane (8, 10). Others have demonstrated upregulation of genes in this pathway in response to acid exposure (29, 62), hypoxia (58, 62), and treatment with antibiotics, such as clofazamine and rifapentine (7). Furthermore, *M. tuberculosis* strains with de-

TABLE 2 Metabolites identified as statistically significantly more abundant in both *rpoB* mutants versus wild-type parent strains of *M. tuberculosis*, with putative identifications

Mass (M+H)[+]	RT[a] (s)	Avg peak intensity		P value	Avg peak intensity		P value
		Haarlem rpoB	Haarlem WT		Beijing rpoB	Beijing WT	
Spectra in chloroform fraction identified as diacylglycerol phosphocholine-related polymer[b] (score[c] = 3)							
200.1	318	11.598	4.620	0.043	6.580	3.204	0.001
215.1	318	217.697	89.613	0.050	126.643	62.609	0.001
747.6	318	444.030	189.220	0.048	243.566	119.076	0.001
819.7	318	74.700	31.109	0.048	41.029	25.357	0.015
838.7	318	54.247	17.966	0.046	26.170	11.222	0.001
780.6	487	31.377	20.849	0.044	126.434	63.609	0.032
807.6	517	110.520	69.352	0.041	396.873	59.912	0.000
808.6	517	40.775	27.568	0.049	127.011	25.237	0.000
864.8	693	3,945.021	3,202.000	0.007	5,929.751	3,489.109	0.000
865.8	693	2,079.054	1,681.559	0.008	4,001.476	2,100.497	0.000
Spectra in chloroform fraction identified as a PDIM derivative[d] (score = 1)							
797.7	679	291.565	236.479	0.043	1,281.437	607.982	0.000
823.2	679	6.644	4.660	0.043	34.537	21.806	0.008
Spectra in methanol fraction identified as a Hex-*N*-acetyl-hexosamine-fucose-*N*-acetyl-hexosamine-related polymer[a] (score = 3)							
321.2	1,016	60.948	46.177	0.047	42.502	29.030	0.003
567.4	1,016	98.960	63.557	0.025	56.887	33.203	0.014
636.5	1,016	48.163	32.947	0.048	29.572	14.773	0.011
637.5	1,016	16.337	7.594	0.038	9.879	3.414	0.020
717.6	1,016	8,520.133	6,005.559	0.048	5,015.322	2,481.935	0.002
719.6	1,016	631.562	470.320	0.043	439.111	292.037	0.027
736.6	1,016	126.813	87.716	0.017	359.462	193.015	0.007
754.6	1,016	224.169	158.316	0.047	139.541	79.460	0.004
771.6	1,016	408.037	265.790	0.049	226.849	117.176	0.005
880.6	1,016	15.607	6.143	0.024	8.211	2.613	0.005
Spectra in methanol fraction identified as a PG derivative[e] (score = 2)							
187.1	1,061	208.350	143.458	0.016	160.662	110.637	0.011
265.1	1,061	21.793	13.452	0.028	17.680	12.084	0.027
345.2	1,061	10.419	5.687	0.034	14.349	5.727	0.019
363.2	1,061	74.866	49.437	0.014	63.242	44.048	0.003
389.3	1,061	53.262	34.879	0.024	46.866	31.877	0.017
531.5	1,061	151.562	91.939	0.036	109.917	56.560	0.015
532.5	1,061	56.525	36.064	0.028	42.000	20.758	0.012
636.5	1,061	47.548	23.712	0.004	38.509	17.748	0.009
699.6	1,061	33.271	18.839	0.023	24.653	12.342	0.021
717.6	1,061	6,257.378	3,655.220	0.033	4,529.182	1,897.650	0.007
718.6	1,061	2,867.806	1,806.767	0.045	2,124.351	1,002.772	0.008
735.6	1,061	799.634	409.858	0.034	546.444	249.317	0.014
736.6	1,061	83.305	52.974	0.030	249.131	128.015	0.011
753.6	1,061	170.532	104.240	0.038	123.990	62.392	0.007
754.6	1,061	94.545	61.712	0.036	71.979	43.733	0.031
771.6	1,061	198.991	117.007	0.014	131.692	70.860	0.007
772.6	1,061	107.522	67.597	0.009	80.007	42.733	0.016
773.6	1,061	31.654	18.005	0.015	22.130	11.537	0.025
789.6	1,061	247.516	151.338	0.036	177.175	94.146	0.015
790.6	1,061	124.074	79.885	0.024	91.662	53.478	0.013
791.6	1,061	37.056	23.549	0.046	27.228	15.857	0.012
807.6	1,061	296.842	176.814	0.033	201.738	97.621	0.008
808.6	1,061	166.267	93.964	0.015	109.848	52.227	0.022
809.6	1,061	52.777	30.453	0.030	36.652	20.813	0.017

[a] RT, retention time.

[b] Identified by analysis in LipidMaps or Massbank.

[c] Scoring system based on metabolite identification guidelines (http://www.metabolomicssociety.org). Scores: 1, identified compound where the retention time and mass spectrum of interest match those of a purified standard; 2, putatively annotated compound based on spectral similarity to public spectral libraries or published data; 3, putatively characterized compound classes based on spectral similarity to known compounds of a chemical class.

[d] Identified by comparison of MS spectra produced by analysis of purified PDIM from *M. tuberculosis*.

[e] Identified by query of published reports of *M. tuberculosis* peptidoglycan (PG) mass spectra.
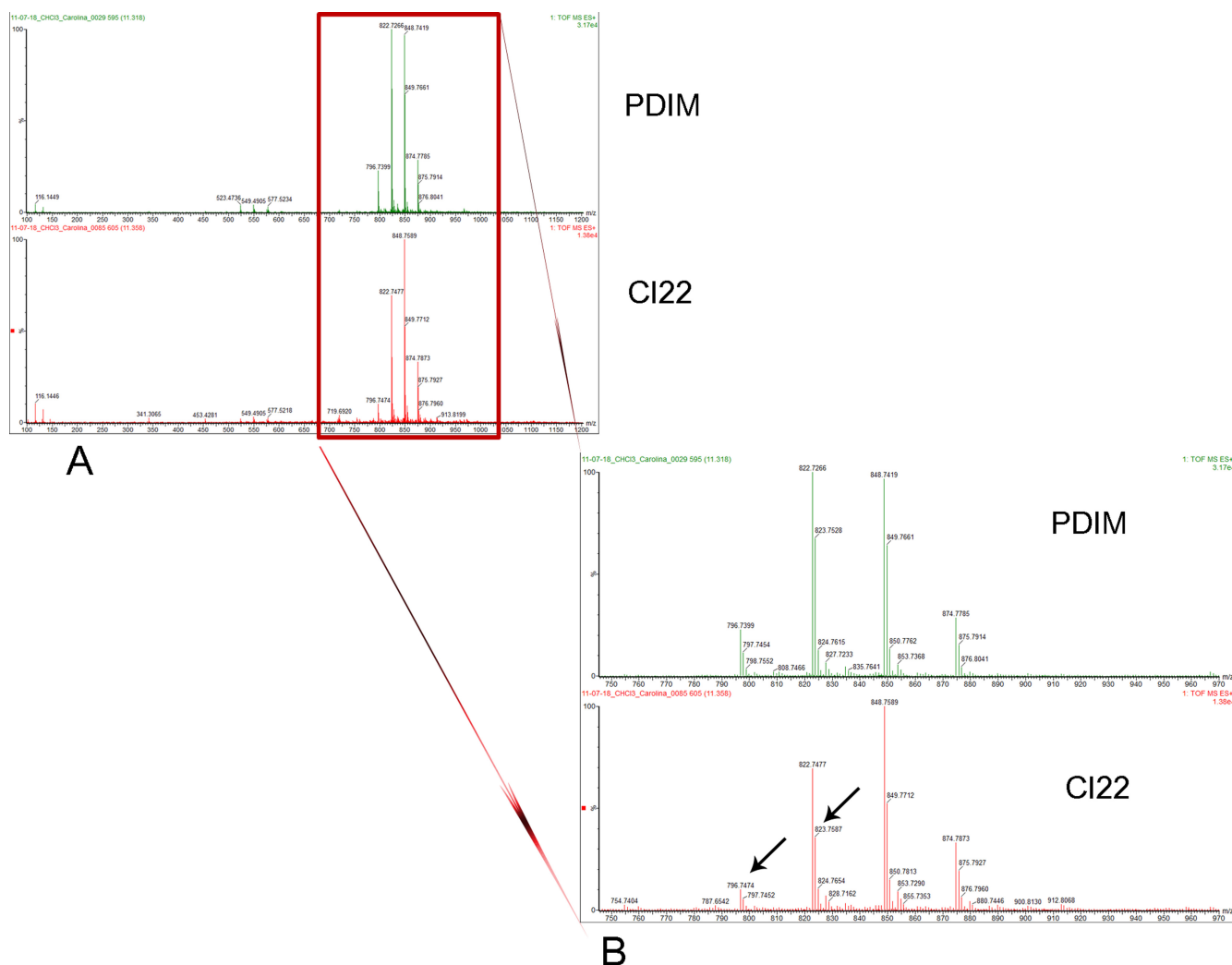
FIG 3 Representative spectra for some of the significant features found at higher abundance in the chloroform fraction of *rpoB* mutant versus WT susceptible *M. tuberculosis* isolates, which also matched peaks found in the PDIM standard. The retention time for these peaks was 11.32 min. The main differentially significant peaks are indicated by arrows (*m/z* 797.7 and *m/z* 823.2). CI22 is the Beijing *rpoB* mutant.

fects in this pathway have been shown to have increased cell envelope permeability (10) and are more susceptible to IFN-γ-mediated and IFN-γ-independent immunity (46, 56). Importantly, PDIM deficiency appears to be particularly important to *M. tuberculosis* growth in the host environment, as isolates with deficiencies in this pathway have pronounced growth defects in the spleens and lungs of infected mice (11, 19, 47) and are more susceptible to the nitric oxide-dependent killing of macrophages (61). More recently, PDIM has been shown to play a role in *M. tuberculosis* interaction with the host macrophage cell envelope, inducing changes that favor receptor-mediated phagocytosis of the bacterium (2). In this study, we found that the upregulation of PDIM by *rpoB* mutants relative to WT isolates, initially identified by proteomics experiments on *M. tuberculosis* isolates grown in broth, was more dramatic when these comparisons were performed in activated murine macrophages. Thus, although we cannot discern the physiological importance of PDIM upregulation by *rpoB* mutants from these data, it is possible that upregulation of

the PDIM pathway is related to increased pressure for *rpoB* mutants to maintain or remodel the cell wall, particularly during host cell infection. Of note, certain other bacteria have been shown to increase lipid abundance in association with *rpoB* mutations, which suggests that this may be a conserved response to the development of drug resistance (73).

The finding of increased peptidoglycan precursors in the *rpoB* mutants in the metabolomics data is also supportive of this hypothesis. Peptidoglycan biosynthesis is a multienzyme process that involves the MurA-MurG cluster, in addition to MurX and a putative flippase (16). Our proteomic analysis identified three of the seven Mur proteins (MurD-MurF) in the cell wall, membrane, and cytosol that did not show significant differences in their abundances between resistant and susceptible strains. However, given the lack of data on the relative abundances of the other peptidoglycan biosynthetic enzymes and the complex nature of peptidoglycan precursor biosynthesis, we cannot discard the idea that the increased amount of PG-related metabolites could be associated

with an increase in the production of PG enzymes, especially with those involved in the last steps of the biosynthetic pathway, such as MurG and MurX (also known as MraY). Further work is required to evaluate this possibility, however. Nonetheless, peptidoglycan and PDIM are both significant components of the cell envelope, with peptidoglycan forming the inner cell wall layer and PDIM decorating the outer layer via noncovalent association with other cell envelope lipids (9). Peptidoglycan interacts (at least indirectly) with PDIM to form the mature mycobacterial cell envelope, in that PDIM translocates across peptidoglycan via *mmpl7* to reside in the outer layer of the cell envelope (39).Thus, it is plausible that changes in PG ultrastructure combined with changes in PDIM biosynthesis synergize to affect the overall integrity of the mycobacterial cell envelope together in response to *rpoB* mutation.

rpoB mutant strains of saprophytic environmental mycobacteria have been found to cohabit with rifamycin-producing organisms on marine sponges (38), indicating that ancestors of *M. tuberculosis* faced rifamycin exposure long before this class of antibiotics was used to treat TB. Rifamycin-resistant *rpoB* mutant environmental mycobacteria antagonized by antibiotics secreted by surrounding competitor organisms conceivably would have experienced a survival advantage if they were able to maintain the integrity of their cell walls. Thus, it is possible that upregulation of the PDIM biosynthetic pathway in *rpoB* mutants of *M. tuberculosis*, as demonstrated here in both broth and macrophage culture, is a defense mechanism response to competition interference inherited from the environmental ancestors of *M. tuberculosis*. Although the physiological relevance of this gene upregulation to the human pathogen *M. tuberculosis* is unknown, it may be important to the survival of rifampin-resistant mycobacteria in the setting of rifamycin or other antibiotic exposure. In particular, future research should comprehensively investigate the degrees to which various globally heterogeneous strains of *rpoB* mutant *M. tuberculosis* upregulate PDIM, the mechanisms that result in PDIM upregulation, and the effect of *rpoB* mutation and PDIM upregulation on susceptibility to various stressors, including existing and novel antibiotics used to treat TB.

The *M. tuberculosis* genome contains an expansive repertoire of polyketide synthase genes that in related bacteria are involved in the biosynthesis of various secondary metabolites, including erythromycin A and rifamycin B (17, 28, 57). The finding of upregulation of several genes encoding polyketide synthases in both *rpoB* mutants of *M. tuberculosis* is of interest in that it suggests that the adaptive response of *M. tuberculosis* to *rpoB* mutation may be analogous to responses observed in related model organisms. As such, *rpoB* mutations lead to upregulation of otherwise dormant gene clusters, resulting in increased abundance of specific secondary metabolites that are absent or minimally present in wild-type strains (34, 79). For example, genes encoding protein enzymes involved in actinorhodin (Act) and undecylprodigiosin (Red) biosynthesis are found in *Streptomyces lividans* but normally are not expressed by the corresponding paired wild-type isolates from which they arose (35). Certain rifampin-resistant *rpoB* mutants of *S. lividans*, however, produce both Act and Red in abundance, a phenomenon that can be reversed by replacing mutant with wild-type *rpoB* (35). Similarly, specific *rpoB* mutations in *Bacillus subtilis* lead to dramatic autoinduction of the antibiotic 3,3′-neotrehalosadiame (NTD), which wild-type strains do not produce (37). Remarkably, while only certain *rpoB* mutations are associated

with gene upregulation in model organisms, the specific mutations most commonly associated with induced gene expression in nonmycobacterial organisms (13, 35, 37) align with mutations most commonly found in clinical rifampin-resistant *M. tuberculosis* strains (i.e., positions 445 and 450 in *M. tuberculosis*) (15, 32, 54, 70, 78). This suggests that those *rpoB* mutations that trigger upregulation of genes involved in biosynthesis of secondary metabolites are evolutionarily advantageous.

Camacho et al. demonstrated that the PDIM locus is divided into three transcriptional units, one spanning *fadD26* to *papA5* (which includes the genes *ppsA-ppsE* and *drrA*), another containing only the *mas* gene, and a third including *fadD28* and *mmpL7* (10). The transcription of all three units appears to be required for the correct biosynthesis and placement of intact PDIM in the cell (10). The genes *ppsC*, *ppsE*, and *drrA* are located within the first transcriptional unit, and in this study, their corresponding PDIM precursor proteins were detected at statistically significantly higher levels in the *rpoB* mutants than in their corresponding wild-type parent strains. Although the limited sensitivity of shotgun proteomics approaches hinders our ability to definitively conclude that proteins found in the other two downstream PDIM transcriptional units were not also upregulated, these findings, together with the metabolomics data, suggest that the first transcriptional unit of the PDIM biosynthetic locus, and not the others, may be specifically upregulated in *rpoB* mutant isolates of *M. tuberculosis*. Comprehensive transcriptomics data are needed to confirm this hypothesis, and if it is true, the biological relevance of this phenomenon is unknown. PDIM production is characteristic of pathogenic, but not environmental, mycobacterial strains (20). This indicates that PDIM production is not important for survival of environmental mycobacteria and, to the extent that the responses of *M. tuberculosis* to *rpoB* mutation may have been inherited from the saprophytic environmental ancestors of *M. tuberculosis*, provides one speculative explanation for the observation that intact PDIM was not found in greater amounts in *rpoB* mutant isolates in this study.

Domenech and Reed have shown that *in vitro* passage of *M. tuberculosis* H37Rv can lead to the inability of mycobacteria to produce PDIM (21). However, the two H37Rv strains analyzed (ATCC versus Pasteur) showed significant differences in the appearance of the PDIM phenotype, which may indicate that loss of PDIM can be affected by the strain genetic background. In the present study, clinical isolates from two different *M. tuberculosis* genotypes had minimal *in vitro* passage, and all of them showed the presence of PDIM when assessed by TLC (see Fig. S1 in the supplemental material). From these isolates, only the *rpoB* mutants showed higher abundance of Pps proteins and of a PDIM-related fragment or precursor, suggesting these changes are directly related to the *rpoB* mutations rather than spontaneous mutations acquired during *in vitro* culture. Analysis of the whole genome sequences of these isolates will add important information and may provide additional explanations for the findings reported in the present study.

This comprehensive analysis suggests that further research to identify more precisely the effects of *rpoB* mutation on gene expression in *M. tuberculosis* will yield novel insights into diagnostics and treatments for drug-resistant TB. For example, if induction of PDIM biosynthetic pathways represents a compensatory virulence mechanism as a result of *rpoB* mutation, the development of novel drugs specifically targeting these pathways may be particu-

larly effective when used to treat TB caused by rifampin-resistant *M. tuberculosis*. Although the *ppsA-ppsE* genes are considered nonessential by transposon mutagenesis (64), Camacho et al. showed that mutant strains of *M. tuberculosis* with transposon insertions in the PDIM biosynthetic pathway were more sensitive to detergents than wild-type strains (10). Thus, growth of *rpoB* mutants may be more sensitive to inhibitors of this pathway than wild-type strains, but this hypothesis remains to be tested. Furthermore, if certain genes are expressed preferentially by rifampin-resistant *M. tuberculosis* strains, immune responses to the corresponding proteins could be investigated as a way to identify individuals with rifampin-resistant latent *M. tuberculosis* infection. The significance of gene upregulation associated with *rpoB* mutation for treatment of drug-resistant TB is unknown, but these data indicate that compensatory mechanisms and pathways should be further explored in order to identify new ways to diagnose and treat this globally important disease.

ACKNOWLEDGMENTS

REFERENCES

1. **Ahmad Z, et al.** 2009. Biphasic kill curve of isoniazid reveals the presence of drug-tolerant, not drug-resistant, Mycobacterium tuberculosis in the guinea pig. J. Infect. Dis. **200**:1136–1143.
2. **Astarie-Dequeker C, et al.** 2009. Phthiocerol dimycocerosates of M. tuberculosis participate in macrophage invasion by inducing changes in the organization of plasma membrane lipids. PLoS Pathog. **5**:e1000289. doi:10.1371/journal.ppat.1000289.
3. **Azad AK, Sirakova TD, Fernandes ND, Kolattukudy PE.** 1997. Gene knockout reveals a novel gene cluster for the synthesis of a class of cell wall lipids unique to pathogenic mycobacteria. J. Biol. Chem. **272**:16741–16745.
4. **Barnes PF, et al.** 1989. Characterization of T cell antigens associated with the cell wall protein-peptidoglycan complex of Mycobacterium tuberculosis. J. Immunol. **143**:2656–2662.
5. **Bergval IL, Klatser PR, Schuitema AR, Oskam L, Anthony RM.** 2007. Specific mutations in the Mycobacterium tuberculosis rpoB gene are associated with increased dnaE2 expression. FEMS Microbiol. Lett. **275**:338–343.
6. **Blanchard JS.** 1996. Molecular mechanisms of drug resistance in Mycobacterium tuberculosis. Annu. Rev. Biochem. **65**:215–239.
7. **Boshoff HI, et al.** 2004. The transcriptional responses of Mycobacterium tuberculosis to inhibitors of metabolism: novel insights into drug mechanisms of action. J. Biol. Chem. **279**:40174–40184.
8. **Braibant M, Gilot P, Content J.** 2000. The ATP binding cassette (ABC) transport systems of Mycobacterium tuberculosis. FEMS Microbiol. Rev. **24**:449–467.
9. **Brennan PJ.** 2003. Structure, function, and biogenesis of the cell wall of Mycobacterium tuberculosis. Tuberculosis (Edinb.) **83**:91–97.
10. **Camacho LR, et al.** 2001. Analysis of the phthiocerol dimycocerosate locus of Mycobacterium tuberculosis. Evidence that this lipid is involved in the cell wall permeability barrier. J. Biol. Chem. **276**:19845–19854.
11. **Camacho LR, Ensergueix D, Perez E, Gicquel B, Guilhot C.** 1999. Identification of a virulence gene cluster of Mycobacterium tuberculosis by signature-tagged transposon mutagenesis. Mol. Microbiol. **34**:257–267.
12. **Campbell EA, et al.** 2001. Structural mechanism for rifampicin inhibition of bacterial RNA polymerase. Cell **104**:901–912.
13. **Carata E, et al.** 2009. Phenotypes and gene expression profiles of Saccharopolyspora erythraea rifampicin-resistant (rif) mutants affected in erythromycin production. Microb. Cell Fact. **8**:18.
14. **Carvalho PC, Hewel J, Barbosa VC, Yates JR III.** 2008. Identifying differences in protein expression levels by spectral counting and feature selection. Genet. Mol. Res. **7**:342–356.
15. **Cavusoglu C, Hilmioglu S, Guneri S, Bilgic A.** 2002. Characterization of rpoB mutations in rifampin-resistant clinical isolates of Mycobacterium tuberculosis from Turkey by DNA sequencing and line probe assay. J. Clin. Microbiol. **40**:4435–4438.
16. **Cole ST.** 2005. Tuberculosis and the tubercle bacillus. ASM Press, Washington, DC.
17. **Cole ST, et al.** 1998. Deciphering the biology of Mycobacterium tuberculosis from the complete genome sequence. Nature **393**:537–544.
18. **Comas I, et al.** 2011. Whole-genome sequencing of rifampicin-resistant Mycobacterium tuberculosis strains identifies compensatory mutations in RNA polymerase genes. Nat. Genet. **44**:106–110.
19. **Cox JS, Chen B, McNeil M, Jacobs WR, Jr.** 1999. Complex lipid determines tissue-specific replication of Mycobacterium tuberculosis in mice. Nature **402**:79–83.
20. **Daffe M, Laneelle MA.** 1988. Distribution of phthiocerol diester, phenolic mycosides and related compounds in mycobacteria. J. Gen. Microbiol. **134**:2049–2055.
21. **Domenech P, Reed MB.** 2009. Rapid and spontaneous loss of phthiocerol dimycocerosate (PDIM) from Mycobacterium tuberculosis grown in vitro: implications for virulence studies. Microbiology **155**:3532–3543.
22. **Dreger M.** 2003. Subcellular proteomics. Mass Spectrom. Rev. **22**:27–56.
23. **Fu X, et al.** 2008. Spectral index for assessment of differential protein expression in shotgun proteomics. J. Proteome Res. **7**:845–854.
24. **Gagneux S.** 2009. Fitness cost of drug resistance in Mycobacterium tuberculosis. Clin. Microbiol. Infect. **15**(Suppl. 1):66–68.
25. **Gagneux S, et al.** 2006. The competitive cost of antibiotic resistance in Mycobacterium tuberculosis. Science **312**:1944–1946.
26. **Gandhi NR, et al.** 2010. Multidrug-resistant and extensively drug-resistant tuberculosis: a threat to global control of tuberculosis. Lancet **375**:1830–1843.
27. **Geffen N.** 2010. Cepheid Gene Xpert diagnostic technology for TB. Memories of the 40th World Conference on Lung Health of the International Union Against Tuberculosis and Lung Disease 3–7 December 2009. HIV Treatment Bulletin South (HTB), April 2010 (http://i-base.info/htb-south/960).
28. **Gokhale RS, Saxena P, Chopra T, Mohanty D.** 2007. Versatile polyketide enzymatic machinery for the biosynthesis of complex mycobacterial lipids. Nat. Prod. Rep. **24**:267–277.
29. **Golby P, et al.** 2007. Comparative transcriptomics reveals key gene expression differences between the human and bovine pathogens of the Mycobacterium tuberculosis complex. Microbiology **153**:3323–3336.
30. **Gupta AK, et al.** 2010. Microarray analysis of efflux pump genes in multidrug-resistant Mycobacterium tuberculosis during stress induced by common anti-tuberculous drugs. Microb. Drug Resist. **16**:21–28.
31. **Haas WH, et al.** 1997. Molecular analysis of katG gene mutations in strains of Mycobacterium tuberculosis complex from Africa. Antimicrob. Agents Chemother. **41**:1601–1603.
32. **Herrera L, Jimenez S, Valverde A, Garcia-Aranda MA, Saez-Nieto JA.** 2003. Molecular analysis of rifampicin-resistant Mycobacterium tuberculosis isolated in Spain (1996–2001). Description of new mutations in the rpoB gene and review of the literature. Int. J. Antimicrob. Agents **21**:403–408.
33. **Horai H, et al.** 2010. MassBank: a public repository for sharing mass spectral data for life sciences. J. Mass Spectrom. **45**:703–714.
34. **Hosaka T, et al.** 2009. Antibacterial discovery in actinomycetes strains with mutations in RNA polymerase or ribosomal protein S12. Nat. Biotechnol. **27**:462–464.
35. **Hu H, Zhang Q, Ochi K.** 2002. Activation of antibiotic biosynthesis by specified mutations in the rpoB gene (encoding the RNA polymerase beta subunit) of Streptomyces lividans. J. Bacteriol. **184**:3984–3991.
36. **Huber LA, Pfaller K, Vietor I.** 2003. Organelle proteomics: implications for subcellular fractionation in proteomics. Circ. Res. **92**:962–968.
37. **Inaoka T, Takahashi K, Yada H, Yoshida M, Ochi K.** 2004. RNA polymerase mutation activates the production of a dormant antibiotic 3,3′-neotrehalosadiamine via an autoinduction mechanism in Bacillus subtilis. J. Biol. Chem. **279**:3885–3892.
38. **Izumi H, et al.** 2010. Diversity of Mycobacterium species from marine sponges and their sensitivity to antagonism by sponge-derived rifamycin-synthesizing actinobacterium in the genus Salinispora. FEMS Microbiol. Lett. **313**:33–40.
39. **Jain M, Cox JS.** 2005. Interaction between polyketide synthase and transporter suggests coupled synthesis and export of virulence lipid in M. tuberculosis. PLoS Pathog. **1**:e2. doi:10.1371/journal.ppat.0010002.

40. **Jain M, et al.** 2007. Lipidomics reveals control of Mycobacterium tuberculosis virulence lipids via metabolic coupling. Proc. Natl. Acad. Sci. U. S. A. **104**:5133–5138.

41. **Jin DJ, Gross CA.** 1988. Mapping and sequencing of mutations in the Escherichia coli rpoB gene that lead to rifampicin resistance. J. Mol. Biol. **202**:45–58.

42. **Kall L, Storey JD, MacCoss MJ, Noble WS.** 2008. Assigning significance to peptides identified by tandem mass spectrometry using decoy databases. J. Proteome Res. **7**:29–34.

43. **Karakousis PC, Williams EP, Bishai WR.** 2008. Altered expression of isoniazid-regulated genes in drug-treated dormant Mycobacterium tuberculosis. J. Antimicrob. Chemother. **61**:323–331.

44. **Karakousis PC, et al.** 2004. Dormancy phenotype displayed by extracellular Mycobacterium tuberculosis within artificial granulomas in mice. J. Exp. Med. **200**:647–657.

45. **Keller A, Nesvizhskii AI, Kolker E, Aebersold R.** 2002. Empirical statistical model to estimate the accuracy of peptide identifications made by MS/MS and database search. Anal. Chem. **74**:5383–5392.

46. **Kirksey MA, et al.** 2011. Spontaneous phthiocerol dimycocerosate-deficient variants of Mycobacterium tuberculosis are susceptible to gamma interferon-mediated immunity. Infect. Immun. **79**:2829–2838.

47. **Kondo E, Kanai K.** 1976. A suggested role of a host-parasite lipid complex in mycobacterial infection. Jpn. J. Med. Sci. Biol. **29**:199–210.

48. **Lavollay M, et al.** 2008. The peptidoglycan of stationary-phase Mycobacterium tuberculosis predominantly contains cross-links generated by L,D-transpeptidation. J. Bacteriol. **190**:4360–4366.

49. **Li MH, Ung PM, Zajkowski J, Garneau-Tsodikova S, Sherman DH.** 2009. Automated genome mining for natural products. BMC Bioinformatics **10**:185.

50. **Lonnroth K, et al.** 2010. Tuberculosis control and elimination-50: cure, care, and social development. Lancet **375**:1814–1829.

51. **Louw GE, et al.** 2011. Rifampicin reduces susceptibility to ofloxacin in rifampin-resistant Mycobacterium tuberculosis through efflux. Am. J. Respir. Crit. Care Med. **184**:269–276.

52. **Mahapatra S, Scherman H, Brennan PJ, Crick DC.** 2005. N glycosylation of the nucleotide precursors of peptidoglycan biosynthesis of Mycobacterium spp. is altered by drug treatment. J. Bacteriol. **187**:2341–2347.

53. **Manganelli R, Dubnau E, Tyagi S, Kramer FR, Smith I.** 1999. Differential expression of 10 sigma factor genes in Mycobacterium tuberculosis. Mol. Microbiol. **31**:715–724.

54. **Mani C, Selvakumar N, Narayanan S, Narayanan PR.** 2001. Mutations in the rpoB gene of multidrug-resistant Mycobacterium tuberculosis clinical isolates from India. J. Clin. Microbiol. **39**:2987–2990.

55. **Mehaffy C, et al.** 2010. Descriptive proteomic analysis shows protein variability between closely related clinical isolates of Mycobacterium tuberculosis. Proteomics **10**:1966–1984.

56. **Murry JP, Pandey AK, Sassetti CM, Rubin EJ.** 2009. Phthiocerol dimycocerosate transport is required for resisting interferon-gamma-independent immunity. J. Infect. Dis. **200**:774–782.

57. **Parish T, Brown A.** 2009. Mycobacterium: genomics and molecular biology. Caister Academic Press, Norfolk, United Kingdom.

58. **Park HD, et al.** 2003. Rv3133c/dosR is a transcription factor that mediates the hypoxic response of Mycobacterium tuberculosis. Mol. Microbiol. **48**:833–843.

59. **Reed MB, et al.** 2004. A glycolipid of hypervirulent tuberculosis strains that inhibits the innate immune response. Nature **431**:84–87.

60. **Rouse DA, Li Z, Bai GH, Morris SL.** 1995. Characterization of the katG and inhA genes of isoniazid-resistant clinical isolates of Mycobacterium tuberculosis. Antimicrob. Agents Chemother. **39**:2472–2477.

61. **Rousseau C, et al.** 2004. Production of phthiocerol dimycocerosates protects Mycobacterium tuberculosis from the cidal activity of reactive nitrogen intermediates produced by macrophages and modulates the early immune response to infection. Cell Microbiol. **6**:277–287.

62. **Rustad TR, Harrell MI, Liao R, Sherman DR.** 2008. The enduring hypoxic response of Mycobacterium tuberculosis. PLoS One **3**:e1502. doi:10.1371/journal.pone.0001502.

63. **Sartain MJ, Slayden RA, Singh KK, Laal S, Belisle JT.** 2006. Disease state differentiation and identification of tuberculosis biomarkers via native antigen array profiling. Mol. Cell. Proteomics **5**:2102–2113.

64. **Sassetti CM, Boyd DH, Rubin EJ.** 2003. Genes required for mycobacterial growth defined by high density mutagenesis. Mol. Microbiol. **48**:77–84.

65. **Shah NS, et al.** 2007. Worldwide emergence of extensively drug-resistant tuberculosis. Emerg. Infect. Dis. **13**:380–387.

66. **Smith CA, et al.** 2005. METLIN: a metabolite mass spectral database. Ther. Drug Monit. **27**:747–751.

67. **Subramanian A, et al.** 2005. Gene set enrichment analysis: a knowledge-based approach for interpreting genome-wide expression profiles. Proc. Natl. Acad. Sci. U. S. A. **102**:15545–15550.

68. **Takayama K, Wang L, David HL.** 1972. Effect of isoniazid on the in vivo mycolic acid synthesis, cell growth, and viability of Mycobacterium tuberculosis. Antimicrob. Agents Chemother. **2**:29–35.

69. **Tala A, et al.** 2009. Activation of dormant bacterial genes by Nonomuraea sp. strain ATCC 39727 mutant-type RNA polymerase. J. Bacteriol. **191**:805–814.

70. **Telenti A, et al.** 1993. Detection of rifampicin-resistance mutations in Mycobacterium tuberculosis. Lancet **341**:647–650.

71. **Thayil SM, Morrison N, Schechter N, Rubin H, Karakousis PC.** 2011. The role of the novel exopolyphosphatase MT0516 in Mycobacterium tuberculosis drug tolerance and persistence. PLoS One **6**:e28076. doi:10.1371/journal.pone.0028076.

72. **Trivedi OA, et al.** 2005. Dissecting the mechanism and assembly of a complex virulence mycobacterial lipid. Mol. Cell **17**:631–643.

73. **Vitali B, et al.** 2008. Molecular and phenotypic traits of in-vitro-selected mutants of Bifidobacterium resistant to rifaximin. Int. J. Antimicrob. Agents **31**:555–560.

74. **Vizcaino JA, et al.** 2010. The Proteomics Identifications database: 2010 update. Nucleic Acids Res. **38**:D736–D742.

75. **WHO.** 2010. Global tuberculosis control 2010. World Health Organization, Geneva, Switzerland.

76. **WHO.** 2010. Multi-drug and extensively drug-resistant TB (M/XDR-TB): 2010 global report on surveillance and response. World Health Organization, Geneva, Switzerland.

77. **Wright A, et al.** 2009. Epidemiology of antituberculosis drug resistance 2002–07: an updated analysis of the Global Project on Anti-Tuberculosis Drug Resistance Surveillance. Lancet **373**:1861–1873.

78. **Yue J, et al.** 2003. Mutations in the rpoB gene of multidrug-resistant Mycobacterium tuberculosis isolates from China. J. Clin. Microbiol. **41**:2209–2212.

79. **Zazopoulos E, et al.** 2003. A genomics-guided approach for discovering and expressing cryptic metabolic pathways. Nat. Biotechnol. **21**:187–190.